Effect of {10–12} twinning on the deformation behavior of AZ31 magnesium alloy

Dewen Hou, Yuzhi Zhu, Qizhen Li, Tianmo Liu, Haiming Wen

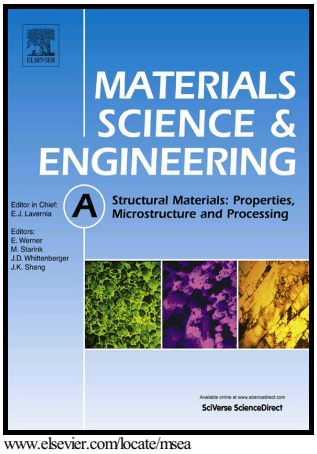

www.elsevier.com/locate/msea

PII: S0921-5093(19)30021-8
DOI: https://doi.org/10.1016/j.msea.2019.01.021
Reference: MSA37421

To appear in: *Materials Science & Engineering A*

Received date: 27 September 2018
Revised date: 20 December 2018
Accepted date: 5 January 2019

Cite this article as: Dewen Hou, Yuzhi Zhu, Qizhen Li, Tianmo Liu and Haiming Wen, Effect of {10–12} twinning on the deformation behavior of AZ31 magnesium alloy, *Materials Science & Engineering A,* https://doi.org/10.1016/j.msea.2019.01.021

Effect of {10-12} twinning on the deformation behavior of AZ31 magnesium alloy

Dewen Hou[a,b], Yuzhi Zhu[a], Qizhen Li[a], Tianmo Liu[b], Haiming Wen[c]

[a]School of Mechanical and Materials Engineering, Washington State University, Pullman, Washington, 99164, USA

[b]School of Materials Science and Engineering, Chongqing University, Chongqing, 400044, China

[c]Department of Materials Science and Engineering, Missouri University of Science and Technology, Rolla, Missouri, 65409, USA

qizhen.li@wsu.edu

wenha@mst.edu

[*]Corresponding author: Tel: +1 509 335 7437.

[*]Corresponding author: Tel: +1 573 341 6167.

Abstract

Twinning process and dislocation characteristics were determined by means of quasi *in-situ* electron backscatter diffraction and high-resolution transmission electron microscopy techniques in a rolled AZ31 magnesium alloy under different strain paths (compression along rolling direction and tension along normal direction). It is demonstrated that the activation of different twin variants depends on the strain path, and thus these twin variants can further induce different texture characteristics. In addition, two independent slip systems were activated during deformation of both strain paths. However, the dislocation slip modes of the two kinds of deformation are different, resulting in different stress-strain response.

Keywords: Twinning; Dislocation slip; Electron backscatter diffraction; High-resolution transmission electron microscopy

1. Introduction

Magnesium alloys are important materials for various technological applications, such as in the automotive components [1, 2], electronic products [3] and aerospace industry [4]. However, magnesium alloys usually have poor mechanical property and a lack of formability, which limits their suitability for many applications [5-8]. Thus, understanding the deformation mechanisms of magnesium alloys is an active area of recent research.

Compared with cubic structures such as face-centered cubic (FCC) and body-centered cubic (BCC), the hexagonal close packing (HCP) structure has lower symmetry that contributes to its deficiency in formability. The most common slip mode reported for the HCP structure is the basal <a> slip [9-11]. However, the basal <a> slip provides only two available independent slip systems, out of the necessary five. Thus, non-basal slip modes including prismatic <a> slip and pyramidal <c+a> slip are required to satisfy the von Misses criterion during plastic deformation [12-16]. In addition to activation of slip systems, twinning is a critical plastic deformation mode for magnesium alloys. In magnesium, the {10-12} tensile twinning mode has been observed frequently at room temperature due to its low critical resolved shear stress (CRSS) [17-19]. This twinning system can be activated under two strain conditions, i.e., compression perpendicular to the c-axis of the HCP unit cell or tension parallel to the c-axis [20-23]. The twinning system can accommodate extension along the c-axis and lead to an 86.3^{o} rotation of the crystal axis around a <11-20> direction [24, 25]. Therefore, in polycrystalline magnesium alloys, the mechanical

response and the evolution of texture during straining are affected by the relationship between initial texture and strain path [24, 25].

For the commonly used wrought magnesium alloys, which have a strong basal texture [26-28], it possible for various deformation behaviors to occur during different strain paths. In a textured magnesium alloy, the directionality of twinning results in strongly anisotropic mechanical behavior [29, 30]. One of the consequences of twinning is that the reorientation of grains can influence subsequent slip [31-33]. Although extensive work has been conducted on twinning behavior in different textured materials and under various loading conditions, the activation of specific slip modes in both matrix and twin in polycrystalline magnesium alloys under different deformation conditions still remains unclear.

In the current work, the twinning behavior and dislocation characteristics of a rolled AZ31 magnesium alloy were investigated under different loading conditions at room temperature. Electron backscatter diffraction (EBSD) orientation examination was performed to observe the evolution of microstructure and crystallographic orientation during the interrupted deformation process, and changes in dislocation types after twinning were observed in details using high-resolution transmission electron microscopy (HRTEM) technique.

2. Experimental procedures

The material employed in the current study was rolled AZ31 (Mg-3%Al-1%Zn, wt%) magnesium alloy sheet. To reduce dislocations or residual stress that might be introduced during sample preparation, the initial material was annealed at 350 ^{o}C for 2 hours. The thickness of initial sheet is 20 mm. Compressive and tensile specimens were machined from the plate along the RD and ND，respectively, as shown in Fig. 1a. Compression tests along the RD were carried out on 10

× 10 × 12 mm^3 (TD × ND × RD) cubes. Tensile tests along the ND were performed on dog-bone shaped specimens with a gage length of 8 mm, a width of 4 mm, and a thickness of 10 mm. The more detailed dimensions of the testing specimens are shown in Fig. 1b and c. A CMT 5150 machine was used for straining. The compressive and tensile samples were loaded in displacement control. Both two tests were carried out at room temperature and at a strain rate of $10^{-3}s^{-1}$.

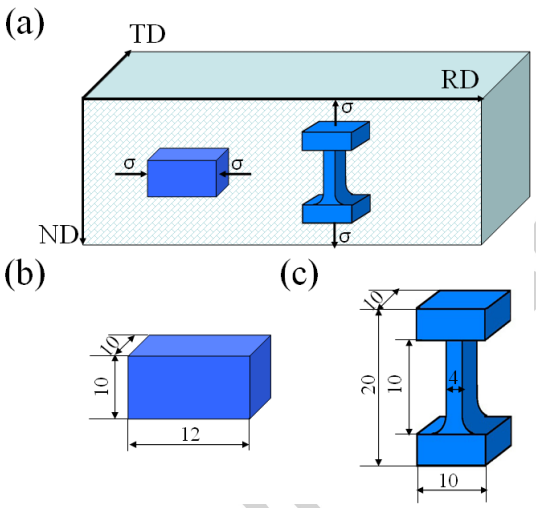

Fig. 1 Schematic configuration showing (a) the rolled sheet and orientations of uniaxial compression and tension samples used in mechanical tests, (b, c) specimen configuration and dimensions.

The microstructure and texture were characterized by a JEOL-7800F scanning electron microscope operated at 20 kV, and the dislocations structure were characterized by a FEI Tecnai TF30 scanning transmission electron microscope operated at 300 kV. Sample preparation for EBSD investigations included sectioning, grinding, mechanical polishing and finally electrochemical polishing with the AC2 commercial electrolyte. The specimens for HRTEM observation were mechanically ground to a finial thickness of ~150 μm, followed by ion-milling

with liquid nitrogen cooling. Accelerating voltages of ion-milling decreased gradually from 5.0 V to 0.5 V and incident angle from 5^{o} to 0.4^{o}.

3. Results and discussion

3.1 Mechanical behavior and microstructure evolution

According to prior reported in the literature [6-33], to ensure the presence of twins in the deformed structures, the uniaxial compressive test was performed to 1.7% strain and the uniaxial tensile test was performed to 2.4% strain, respectively. In order to analyze the microstructure and texture characteristic of the AZ31 magnesium alloy, regions split by boundaries (grains and twins) are distinguished by colors related to their orientations. In theory, twinning is strongly dependent on the initial matrix orientation with respect to the external loading direction: {10-12}<11-20> tensile twin is in favor of nucleation when the c-axis is subjected to a tensile loading, while {10-11}<1-210> contractive twin is in favor of nucleation when the c-axis is subjected to a contractive loading. Thus, in the current work, based on the initial orientation of material and loading directions, only {10-12} tensile twins are considered to be activated. Besides, the twinning deformation also displays a strong grain size and temperature effect [25-30]. In the current work, the materials used in all tests were cut from the same identical rolled sheet. Thus, these factors will be ignored.

Fig. 2 and 3 illustrate the engineering strain-stress curves for room temperature tests performed until failure under compression along RD (Fig. 2) and tension along ND (Fig. 3). In order to confirm the consistency of the results, the test for each strain path was repeated six times to check repeatability. The observed concave-down shape of both strain-stress curves in the early deformation stage is typical for textured magnesium and its alloys under twinning dominated

deformation [27, 30]. Although the early deformations under compression along RD and tension along ND was dominated by the {10-12} tensile twinning, their deformation features in the two deformation modes were different. The yield strength (σ_y) and ultimate strength (σ_{US}) of material during compression along RD are ~ 73 MPa and ~380 MPa, respectively, which are higher than those during tension along ND (σ_y = ~ 64 MPa, and σ_{US} = ~324 MPa), however, the ductility (ε) is lower (~9.5% for compression along RD, and ~ 24.0% for tension along ND).

Generally, there are only two independent slip systems in magnesium alloys, thus theoretically the alloys will exhibit low ductility. However, the two engineering stress-strain curves shown above revealed comparatively good extensibility in both strain paths, which is caused by twinning accormmodation. Here, the strain accommodated by twinning was calculated from the area fractions using the formula [31]:

$$\varepsilon_{\max} = \sqrt{\frac{1}{2}} s V_{twin} \qquad (1)$$

in which s is the twin shear and V_{twin} is the volume fraction of the corresponding twin mode (assumed to be equal to the area fraction of twins).

The characteristics of twins for compression along RD and corresponding texture were shown in Fig. 2a and b. Compared with original microstructure, twins appeared in most of the parent grains after compression, and the twin lamellae generated in a grain almost traversed the grain and are parallel to each other. The textures measured before and after deformation also show very considerable change. It can be observed that the initial basal texture component (c-axis parallel to ND) has weakened and the newly generated RD basal component appeared (c-axis parallel to the RD). These newly generated texture components can be ascribed to {10-12} tensile twinning, which rotates the c-axis by 86.3^o, and the tensile twinning can re-orientate the main

texture component to align with the loading direction.

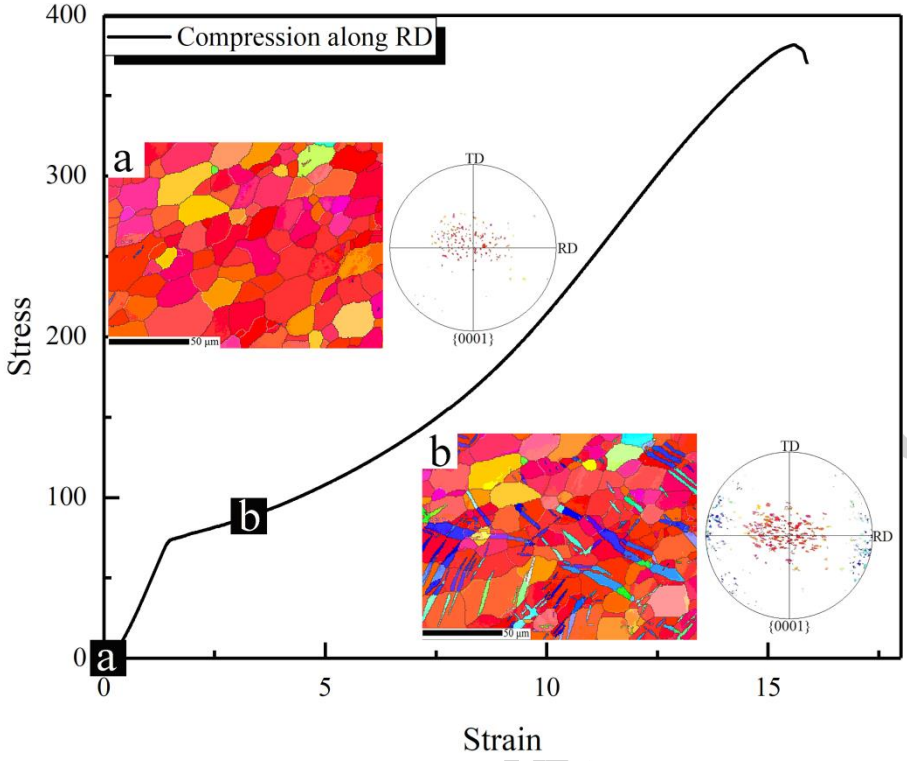

Fig. 2 Engineering stress-strain curve when compressed along RD, and evolution of microstructure and texture in (a) initial sample and (b) sample deformed to 1.7% strain.

Micrographs illustrating the twin characteristics during tension along ND, are presented in Fig. 3. Compared with compression along RD where the twins developed in most grains were parallel to each other, the twins that occurred in a grain were complicated under tensile loading along ND. It was observed that some twin lamellae generated in a grain were parallel to each other and almost traversed the parent grains. However, other parts of twins did not propagate completely across the parent grain: instead, they terminated within the grain or were divided into sections by the matrix or other twins. The formation of such twin characteristics can be illustrated as follows. Tensile twinning can theoretically occur within a grain on any of the six {10-12} planes, and these

twin variants can be presumed to be generated where the resolved shear stress exceeds the critical value τ_c [34-37]. Once more than one twin variant nucleates in a specific parent grain, the following two situations may occur: one twin will be created first, after which the second (or even third) twin will be formed at larger strains; or these variants start to be generated at the same time. In addition, in comparison with the evolution of texture during compression along RD (shown in Fig. 1), it can be observed that new texture components are located symmetrically between RD and TD (c-axis evenly distributed in the plane that is perpendicular to the ND). As noted above, the different characteristics of twined texture are due to the activation of various twin variants under different loading conditions, which will be discussed below.

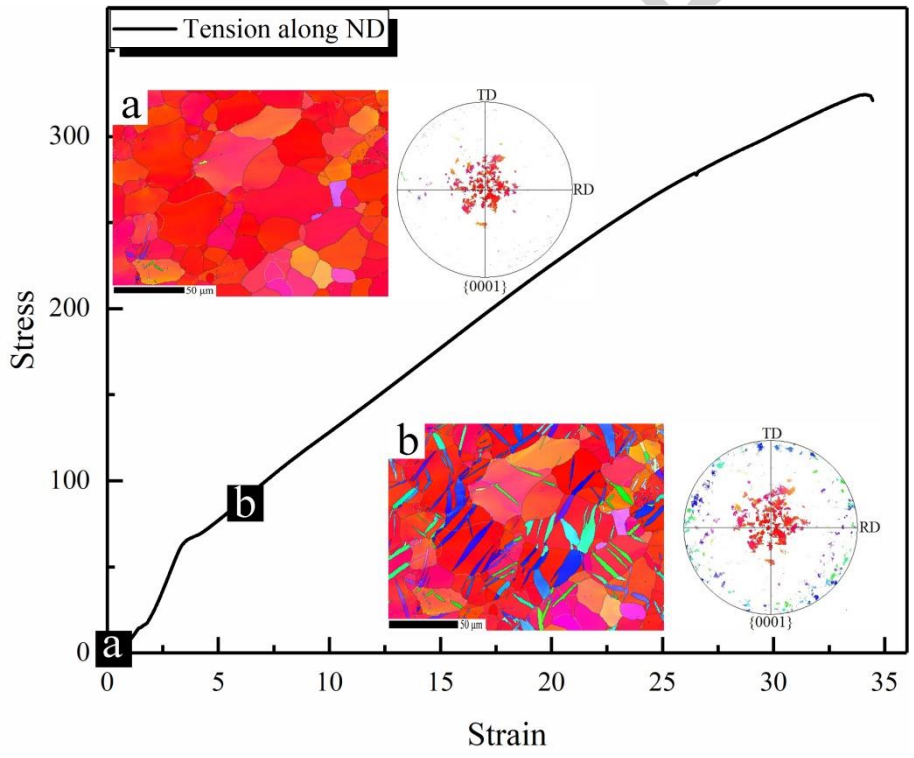

Fig. 3 Engineering stress-strain curve during tension along ND, and evolution of microstructure and texture in (a) initial sample and (b) sample was deformed to 2.4% strain.

Generally, since the local stress concentration is likely to occur at grain boundaries during deformation, twinning begins with the formation of a nucleus that is always located at a grain boundary [38, 39]. Furthermore, with the increase in strain, different twin variants will exhibit different deformation characteristics. For the same twin variants in most grains that always occur in parallel relationship, they will gradually contact each other, and then merge into one grain until the matrix is completely consumed [23, 39]. On the contrary, for the different twin variants nucleated in a grain that intersect each other, the growth of one twin variant will be limited by other twin variants. Ultimately, the grain will be divided into several small sections by these twin variants [26, 36].

Ideally, tensile twin in magnesium is possible on six equivalent {10-12} twinning planes with a specific shear direction of <10-11> [20], i.e. (10-12)[-1011], (1-102)[-1101], (0-112)[0-111], (-1012)[01-11], (-1102)[10-11], (01-12)[1-101], respectively [40-42]. For convenience of distinction and presentation, the crystallographic orientations of the above six variants are encoded as V1 to V6. For grains, once the matrix orientation is fixed, six theoretical twin variants can be determined. Therefore, by comparing the experimental twin variant orientation with the six calculated variants above and finding the closest match, the twin variant can be identified [34].

To identify activated twin variants more clearly, all Euler pattern maps of two deformed samples were plotted, as shown in Fig. 4a and b. This pattern uses an Euler angle based color scale (i.e., similar colors indicate similar orientations). The overwhelming majority of twins are parallel to each other and have the same color during compression along RD, as shown in Fig. 4a, indicating that they fall into the same variant. Meanwhile, occasionally, two twin variants were observed in some grains (but there is a significant difference in the volume fraction between these

two variants), such as twins in grains 4 and 6 in Fig. 4a. During tensile loading along ND, lots of twins intersect each other and they exhibit the different colors, indicating that the different twin variants were formed during this loading condition, as shown in Fig. 4b. These results suggested that twin variant selection is not random, but quite restricted.

Several grains in which different twin variants were detected in all Euler maps were chosen for further investigation. In addition, four grains are selected as an example to analyze the twin variant, as shown at higher magnification in Fig. 4. The corresponding {0001} pole figures of different grains were also shown below the micrographs. Here, the potential twin variants formed on the {0001} plane for different matrix pole points were shown as the V1 – V6 (red diamond mark in the pole figures). Furthermore, unit cells of twin variants and matrix were displayed in the corresponding pole figures. During compression along RD, in grain 1, there is just one twin variant observed in the matrix, which was equal to the theoretically calculated V2 of the parent grain. On the other side, two twin variants were identified in grain 4, which were equivalent to the V4 (T1) and V5 (T2). However, these two variants are significantly different in size, that is, the nucleation of two variants appears to be sequential rather than simultaneous. During tension along ND, in grain 7, three different variants can be identified according to their orientation, where T1 belonged to the theoretical calculated V3 of the matrix grain, T2 belonged to the V5, and T3 belonged to the V4, respectively. These three twin variants intersect each other. In grain8, four twin bands can be observed in the matrix, and they are seemly parallel to each other. Three of them (T1 that is displayed in light grey) were confirmed to be V2, whereas the other twin lamella (T2 that is displayed in dark green) was confirmed to be V4. This indicates that different twin variant pairs in morphology sometimes exhibit in parallel relationship.

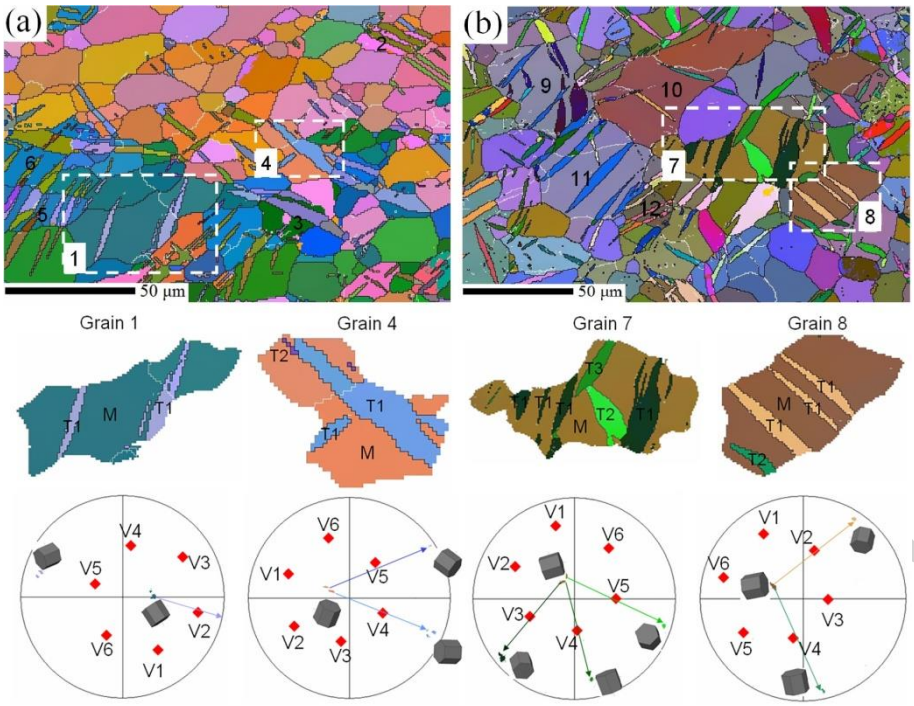

Fig. 4 All Euler maps of two samples under different strain paths: (a) compression along RD, (b) tension along ND.

In order to illustrate the generation of different twin variants during strain path change, Schmid factor (SF) analysis is employed to understand the activated mechanism of different twin variants under two loading conditions. Based on the matrix orientations of selected 12 grains shown in Fig. 4, *m* values of six possible twin variants (see Table 1) were calculated.

For the strain path of compression along RD, comparing the *m* values corresponding to each observed twin in six grains, the most predominant twin variants are found with higher *m* values (the *m* values of activated twin variant are highlighted in red). Here, three aspects should be noted. In the first place, although the *m* values of six variants in grain 1 are relatively low (the highest *m* value is less than 0.3), the twins can still be nucleated. This indicates that tensile twinning can easily be produced during the deformation process. Actually, some researchers have

performed the related calculations in single crystalline magnesium and pointed out that the stress needed to produce the {10-12} tensile twin is quite low (about 2~2.8 MPa) and would be less than 2% of the applied stress [43, 44]. In the second place, twin variants with the first and second highest SFs were observed in grain 4. However, it is easy to see that V4 with the highest *m* value dominates the twinning characteristics. This suggests that when two variants are present in a grain, the one that has larger *m* value is more likely to be nucleated and subsequently grow. In the third place, the *m* values of some twin variants in grains 1, 4, 5, 6 are less than zero, indicating that these variants are in the suppressed state during the twinning process. The activation of twinning is polar and can be activated only when the *m* value is positive [45]. For the strain path of tensile loading along the ND, the *m* values of all six twin variants were relatively high (greater than 0.3 in most grains: see grains 7 - 12 in Table 1). According to the SF criterion, all three twin variant pairs can be possibly activated. However, it is noted that some grains have less than three activated twin variants. These deviations result from the experimental basal texture formed in the initial material which the c-axis of some matrix grains deviated from the ND. Furthermore, due to the fact that c-axis of six twin variants is evenly distributed over the RD – TD plane, the pole point in twined regions is located randomly in the RD – TD plane (as illustrated in Fig. 3) [20]. It can be deduced from the results above that the tensile twinning is mainly governed by the SF criterion. In general, the fact that the different SFs for the two strain paths is the reason for the activation of different twin variants.

Table 1. SF values (*m*) of different twin variants and their activations in the twelve grains in compression and tension specimens.

Grains	*m* values of different twin variants						Activated twin variant
	V1	V2	V3	V4	V5	V6	
1	0.109	0.167	-0.143	0.061	0.113	-0.148	V2
2	0.128	0.498	0.121	0.128	0.499	0.122	V5
3	0.497	0.154	0.097	0.496	0.153	0.098	V4
4	0.344	0.256	-0.025	0.374	0.282	-0.029	V4, V5
5	0.164	0.341	-0.044	0.131	0.297	-0.055	V2
6	0.323	0.361	-0.023	0.3	0.337	-0.024	V2
7	0.42	0.45	0.414	0.382	0.438	0.44	V3, V4, V5
8	0.388	0.394	0.302	0.356	0.41	0.35	V2, V4
9	0.476	0.466	0.47	0.472	0.44	0.448	V3, V4, V5
10	0.252	0.287	0.107	0.21	0.306	0.168	V1, V2
11	0.496	0.497	0.497	0.494	0.487	0.488	V1, V3, V5
12	0.375	0.276	0.347	0.395	0.327	0.378	V4, V5

3.2 Effect of twinning on deformation behavior

As displayed in the section 3.1, different twinning textures were introduced during loading along different directions. Such twinning textures may give rise to different activation of slip systems. To study slip behavior in matrix and twins under two loading conditions, HRTEM

technique was employed to observe the activation of different slip systems. Before that, to better capture dislocation morphology, two samples were deformed to higher strains: the compressive test was performed to 4.8% strain and the tensile test was performed to 6.5% strain. In addition, two main slip systems are considered: basal <a> slip and prismatic <a> slip. Pyramidal <c+a> slip is an optional deformation mode in the magnesium alloy, however, since the critical resolved shear stress of pyramidal slip is much higher than that of basal and prismatic slip at room temperature, pyramidal slip is not be considered in the current work ($CRSS_{basal\ slip}$ = 0.45 ~ 0.81 MPa[46, 47], $CRSS_{prismatic\ slip}$ = 39.2 MPa[48, 49], $CRSS_{pyramidal\ slip}$ = 45 ~ 81 MPa[14, 50]).

Fig. 5a and b show lattice fringe images of matrix and twined regions in a RD compression sample. The inserted fast Flourier transformation (FFT) patterns indicate the misorientation angle between the matrix and twin is about 86^{o}. Inverse FFT analysis of the HRTEM images reveal that <a> dislocations are activated both in matrix and twined regions, as shown in Fig. 5c ~ f. In addition, the average numbers of basal dislocations in matrix and twined regions are approximately equal, but the number of prismatic dislocations in matrix is higher than that in twined region. This indicates that basal slip can be activated easily in the matrix and twined regions, whereas prismatic slip is favored to be activated in the matrix. For tension along ND, HRTEM characterization reveals that a large number of <a> dislocations either on (0002) or (10-10) planes were present, as shown in Fig. 6. Inverse FFT analysis show that the basal dislocations are distributed homogeneously in the matrix and twined regions (Fig. 6c and d). This indicates that basal dislocations are also easily activated under this loading condition. In addition, it can be seen that the number of prismatic slip in matrix is evidently less than that in twined regions (Fig. 6e and f), indicating that prismatic dislocations are more likely to be generated after

twinning.

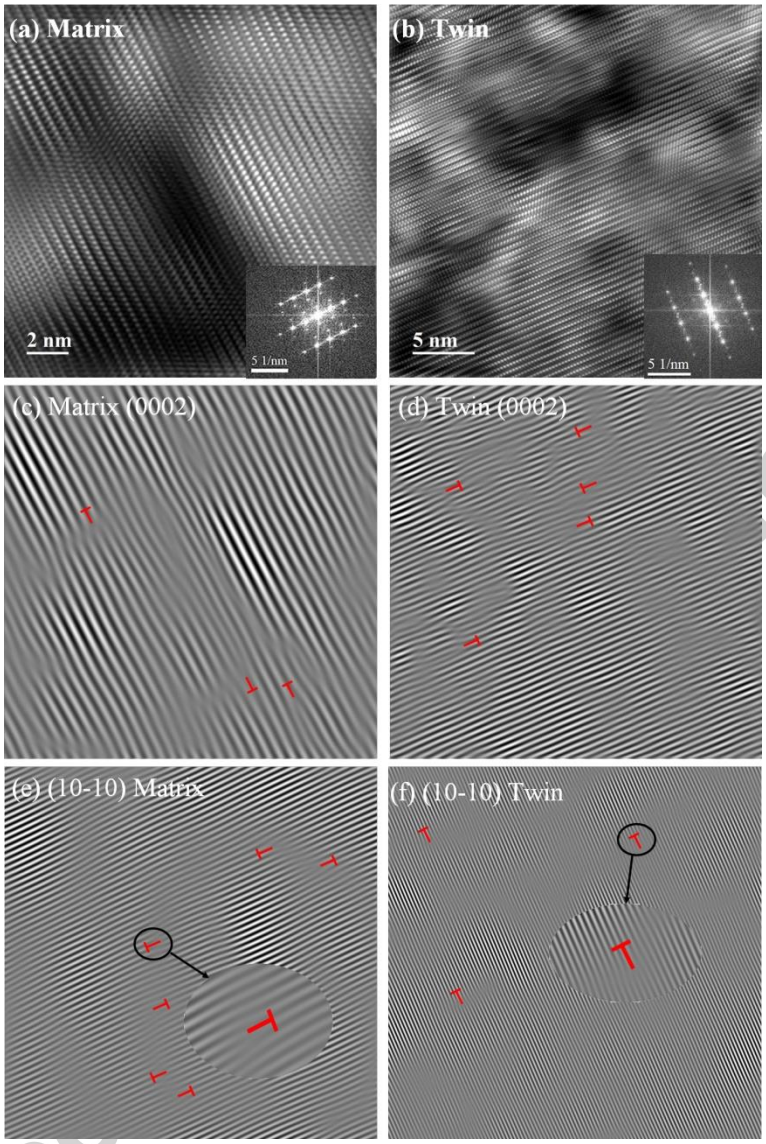

Fig. 5 TEM images for AZ31 magnesium alloy compressed along RD to strain of 4.8%. (a, b) HRTEM images in the matrix and twined regions with the incident beam along [-2110] and their corresponding fast Fourier transform pattern is inserted in the bottom right corner, and inverse Flourier transform patterns for (c, d) (0002) plane for matrix and twin, (d, e) (10-10) plane for matrix and twin. Dislocations are marked with the red “T”.

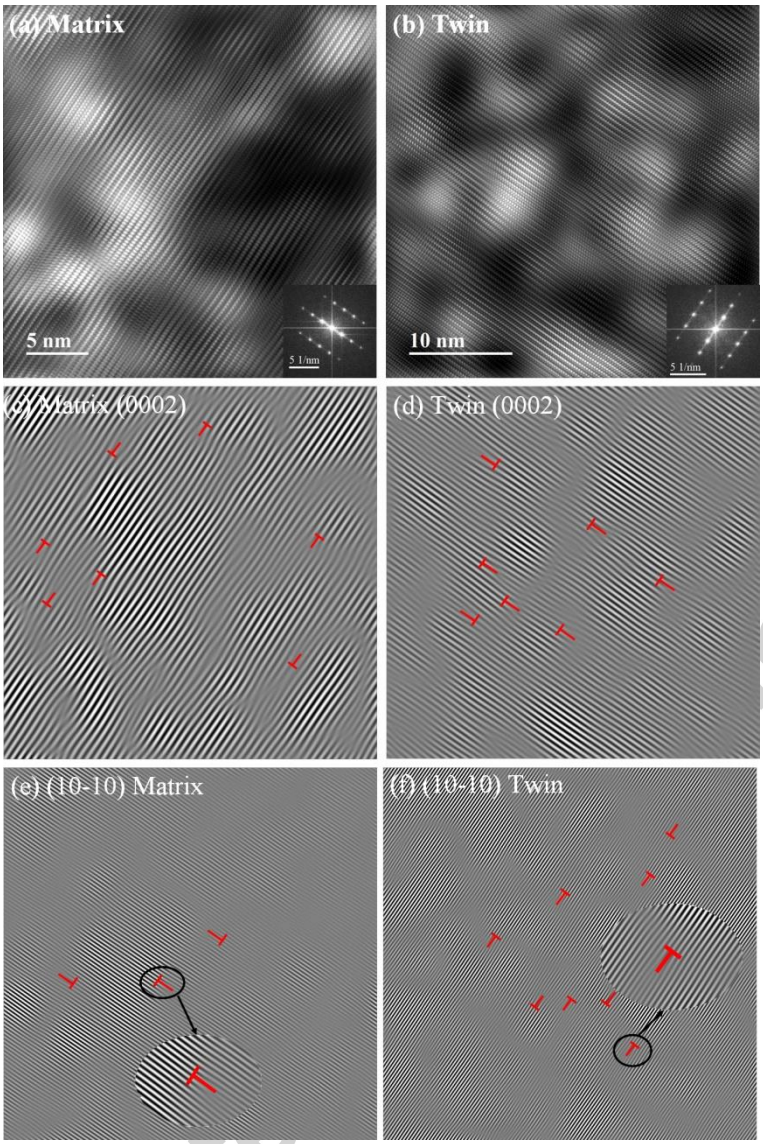

Fig. 6 TEM images for AZ31 magnesium alloy tensile along ND to strain of 6.5%. (a, b) HRTEM images in the matrix and twined regions with the incident beam along [-2110] and their corresponding fast Fourier transform pattern is inserted on the bottom right corner, and inverse Flourier transform image for (c, d) (0002) plane for matrix and twin, (d, e) (10-10) plane for matrix and twin. Dislocations are marked with the red “T”.

Based on the abovementioned observations, in order to better understand the mechanisms of different slip mode activations, the SF distributions of different slip systems in selected 200

matrix grains (one hundred for compression along RD and another hundred from tension along ND) and 200 twins (such as the former) were calculated. In the analysis, due to the fact that the *m* values were dependent upon the angle between the c-axis/a-axis of a set of slip plane/direction and loading directions, it is common to have different *m* values for a slip system. For example, for an orientation from grain 1 in Fig. 4a, where the Euler angle is (φ_1, ϕ, φ_2) = (32.3, 84.2, 31.4) (from the EBSD data), the *m* values of different slip systems under different strain paths can be calculated as shown in Table 2. Hence, it is assumed that only one slip system that has the highest *m* value (m_h) can be activated in a selected slip mode. For the orientation above, $m_h^{basal} = m_{(0001)<-2110>} = 0.449$ and $m_h^{prismatic} = m_{(10-10)<12-10>} = 0.337$ during compression RD, $m_h^{basal} = m_{(0001)<-12-10>} = 0.088$ and $m_h^{prismatic} = m_{(01-10)<-2110>} = 0.44$ during tension along ND.

Table 2. |*m*| values of two main slip systems in a random orientation, (φ_1, ϕ, φ_2) = (95.7, 94.4, 41.6).

Slip modes		|*m*| values	
		Compression along RD	Tension along ND
Basal	(0001)<11-20>	0.19	0.088
	(0001)<-12-10>	0.259	0.086
	(0001)<-2110>	0.449	0.002
Prismatic	(1-100)<11-20>	0.274	0.416
	(10-10)<-12-10>	0.337	0.44
	(01-10)<-2110>	0.063	0.024

*Due to no polarity in the slip, the *m* values of different slip modes take the absolute values.

Fig. 7 shows the distribution of $|m_h|$ values of two slip modes in selected matrix grains and twins under two deformation conditions. For compression along RD (Fig. 7a), the distribution of $|m_h|$ values for basal slip seems dispersed in both matrix grains and twins. In this case, basal <a> slip is favored to be activated. In addition, $|m_h|$ values of prismatic slip in matrix grains are mainly distributed in the range of 0.3 - 0.5 while in twins the values are mainly in the range of 0 - 0.15. This indicates that prismatic <a> dislocations are easier to be activated in matrix than in twins due to their favorable orientations. Thus, for matrix grains in the current studies, the prismatic slip will be limited due to its high CRSS and tensile twinning will be easily activated. For twins, $|m_h|$ values of basal slip are higher than those of prismatic slip. This suggests that the twin texture is still hard to activate prismatic slip and basal slip plays a leading role in this texture. For tension along ND, $|m_h|$ value distributions of basal slip also appear dispersed homogeneously in the matrix grains and twins (Fig. 7b), indicating that basal <a> slip should be activated in the above two textures during tensile deformation. However, $|m_h|$ value distributions of prismatic slip in most matrix grains are mainly concentrated in the range of 0 - 0.2, while in twin texture the values are in the range of 0.4 - 0.5. This indicates that in addition to basal slip and tensile twinning, prismatic <a> slip becomes favorable in twin texture and the contribution of prismatic slip will become more important with the process of tension.

As discussed above, {10-12} tensile twinning can be activated easily in the samples under two loading conditions due to its favorable crystal orientations. In addition to twinning, slips are very significant in both loading conditions. However, the dislocation modes of the two kinds of deformations are quite different, resulting in the distinctively different elongation in the stress-strain curves as shown in Fig. 2 and Fig. 3. Evidently, compared with compression along

RD, the samples under tension along ND show a higher ductility. One of the reasons is the easier activation of prismatic dislocations after twinning during tension along ND, which provides more available independent slip modes during deformation process.

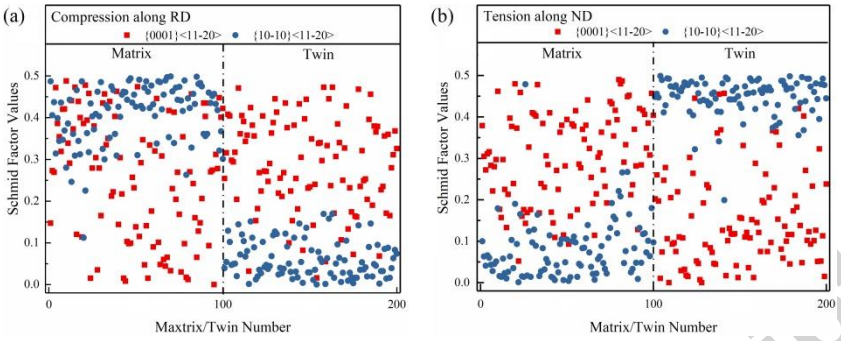

Fig. 7 $|m_h|$ values of different slip systems in selected matrix and twined regions during compression along RD and tension along ND.

4. Conclusions

By quasi *in-situ* EBSD and high-resolution TEM techniques, the activation of tensile twin variants and their effect on the deformation behavior in a rolled AZ31 magnesium alloy have been investigated. The following conclusions are drawn:

(1) Different twinning behavior occurred during different strain paths. During compression along RD, only one twin variant was activated in most grains. However, there are more than two twin variants observed during tension along ND. In addition, twin variant selection is governed by the Schmid factor.

(2) Differences in twinning features between two strain paths resulted in different texture characteristics.

(3) Two independent slip systems were activated during two strain paths deformation.

However, the dislocation modes of the two kinds of deformation are quiet different, finally resulting in distinctively different ductility.

(4) When compression along RD, the basal slip can be activated equally in the matrix and twined regions, whereas prismatic slip is easier to be activated in matrix than in twin regions. When tension along ND, basal dislocations are also easily activated both in the matrix and twined regions, but prismatic dislocations are more likely to be generated after twinning.

Acknowledgments

D. Hou, Y. Zhu, and Q. Li gratefully acknowledge the financial support from the US Department of Energy, Office of Basic Energy Science under Award no. DE-SC0016333.

References

[1] H. Friedrich, S. Schumann. Research for a "new age of magnesium" in the automotive industry. J Mater Process Technol. 117 (3) (2001) 276-281.

[2] M.K. Kulekci. Magnesium and its alloys applications in automotive industry. J Adv Manuf Technol. 39 (9) (2008) 851-865.

[3] T.M. Pollock. Weight loss with magnesium alloy. Science. 328 (2010) 986-987.

[4] D.W. Hou, T.M. Liu, H.C. Chen, D.F. Shi, C.H. Ran, F.S. Pan. Analysis of the microstructure and deformation mechanisms by compression along normal direction in a rolled AZ31 magnesium alloy. Mater Sci Eng A. 660 (2016) 102-107.

[5] W.Q. Xu, N. Birbilis, G. Sha, Y. Wang, J.E. Daniels, Y. Xiao, M. Ferry. A high-specific-strength and corrosion-resistant magnesium alloy. Nature Materials. 14 (2015)

1229-1235.

[6] Q.Z. Li, Q. Yu, J.X. Zhang, Y.Y. Jiang. Effect of strain amplitude on tension-compression fatigue behavior of extruded Mg6Al1ZnA magnesium alloy. Scripta Mater. 62 (2010) 778-781.

[7] M.R. Barnett, A. Ghaderi, J. Quinta da Fonseca, J.D. Robson. Influence of orientation on twin nucleation and growth at low strains in a magnesium alloy. Acta Mater. 80 (2014) 380-391.

[8] S.R. Agnew, Özgür Duygulu. Plastic anisotropy and the role of non-basal slip in magnesium alloy AZ31B. Inter J Plasticity. 21 (2005) 1161-1193.

[9] D.W. Hou, T.M. Liu, M. Shi, H.M. Wen, H.Y. Zhao. Deformation mechanisms in a rolled magnesium alloy under tension along the rolling direction. Microsc Microanal. 24 (2018) 207-213.

[10] Q.Z. Li, Q. Yu, J.X. Zhang, Y.Y. Jiang. Microstructure and deformation mechanism of Mg6Al1ZnA alloy experienced tension-compression cyclic loading. Scripta Mater. 64 (2011) 233-236.

[11] A. Tehranchi, B. Yin, W.A. Curtin. Solute strengthening of basal slip in Mg alloys. Acta Mater. 151 (2018) 56-66.

[12] M.H. Yoo, S. R. Agnew, J.R. Morris, K.M. Ho. Non-basal slip systems in HCP metals and alloys: source mechanisms. Mater Sci Eng A. 319-321 (2001) 87-92.

[13] S. Sandlöbes, M. Friák, J. Neugebauer, D. Raabe. Basal and non-basal dislocation slip in Mg-Y. Mater Sci Eng A. 576 (2013) 61-68.

[14] D.W. Hou, Q.Z. Li, H.M. Wen. Study of reversible motion of {10-12} tensile twin boundaries in a magnesium alloy during strain path changes. Mater Lett. 231 (2018) 84-86.

[15] Q.Z. Li. Mechanical properties and microscopic deformation mechanism of polycrystalline magnesium under high-strain-rate compressive loadings. Mater Sci Eng A. 540 (2012) 130-134.

[16] Q.Z. Li. Dynamic mechanical response of magnesium single crystal under compression loading: experiments, model, and simulations. J Appl Phys. 109 (2011) 103514.

[17] P. Yang, Y. Yu, L. Chen, W. Mao. Experimental determination and theoretical prediction of twin orientation in magnesium alloy AZ31. Scripta Mater. 50 (2004) 1163-1168.

[18] M. Knezevic, A. Levinson, R. Harris, R.K. Mishra, R.D. Doherty, S.U. Kalidindi. Deformation twinning in AZ31: Influence on strain hardening and texture evolution. Acta Mater. 58 (2010) 6230-6242.

[19] A. Khosravani, D.T. Fullwood, B.L. Adams, T.M. Rampton, M.P. Miles, R.K. Mishra. Nucleation and propagation of {10-12} twins in AZ31 magnesium alloy. Acta Mater. 100 (2015) 202-214.

[20] S.G Hong, S.H Park, C.S. Lee. Role of {10-12} twinning characteristics in the deformation behavior of a polycrystalline magnesium alloy. Acta Mater. 58 (2010) 5873-5885.

[21] G.S. Song, S.H. Zhang, L. Zheng, L. Ruan. Twinning, grain orientation and texture variation of AZ31 Mg alloy during compression by EBSD tracing. J Alloys Compd. 509 (2011) 6481-6488.

[22] S.H. Park, S.H. Hong, J.H. Lee, C.S. Lee. Multiple twinning modes in rolled Mg-3Al-1Zn alloy and their selection mechanism. Mater Sci Eng A. 532 (2012) 401-406.

[23] P.D. Wu, X.Q. Guo, H. Qiao, D.J. Lloyd. A constitutive model of twin nucleation, propagation and growth in magnesium crystals. Mater Sci Eng A. 625 (2015) 140-145.

[24] J.B. Shao, Z.Y. Chen, T. Chen, Z. Hu, X.J. Zhou, C.M. Liu. The effect of LPSO on the deformation mechanism of Mg-Gd-Y-Zn-Zr magnesium alloy. J Magnes Alloys. 4 (2016) 83-88.

[25] N. Saikrishna, G. Pradeep Kumar Reddy, B. Munirathinam, B.R. Sunil. Influence of bimodal grain size distribution on the corrosion behavior of friction stir processed biodegradable AZ31 magnesium alloy. J Magnes Alloys. 4 (2016) 68-76.

[26] D.W. Hou, T.M. Liu, L.J. Luo, L.W. Lu, H.C. Chen, D.F. Shi. Twinning behaviors of a rolled AZ31 magnesium alloy under multidirectional loading. Mater Charact. 124 (2017) 122-128.

[27] Q.Z. Li, B. Tian. Mechanical properties and microstructure of pure polycrystalline magnesium rolled by different routes. Mater Lett. 67 (2012) 81-83.

[28] D.W. Hou, T.M. Liu, D.F. Shi, H.C. Chen, H.B. Chen. Study of twinning behaviors of rolled AZ31 magnesium alloy by interrupted in situ compressive tests. Mater Sci Eng A. 653 (2016) 108-114.

[29] A. Chapuis, Y.C. Xin, X.J. Zhou, Q. Liu. {10-12} twin variants selection mechanisms during twinning, re-twinning and detwinning. Mater Sci Eng A. 612 (2014) 431-439.

[30] M.A. Kumar, I.J. Beyerlein, C.N. Tomé. Effect of local stress fields on twin characteristics in HCP metals. Acta Mater. 116 (2016) 143-154.

[31] M. Battaini, E.V. Pereloma, C.H.J. Davies. Orientation effect on mechanical properties of commercially pure titanium at room temperature. Metallurgical and Materials Transactions A. 38A (2007) 276-285.

[32] D. Sarker, D.L. Chen. Dependence of compressive deformation on pre-strain and loading direction in an extruded magnesium alloy texture, twinning and de-twinning. Mater Sci Eng

A. 596 (2014) 134-144.

[33] J. Lind, S.F. Li, R. Pokharel, U. Lienert, A.D. Rollett, R.M. Suter. Tensile twin nucleation events coupled to neighboring slip observed in three dimensions. Acta Mater. 76 (2014) 213-220.

[34] Y. Pei, A. Godfrey, J. Jiang, Y.B. Zhang, W. Liu, Q. Liu. Extension twin variant selection during uniaxial compression of a magnesium alloy. Mater Sci Eng A. 550 (2012) 138-145.

[35] J. Jiang, A. Godfrey, W. Liu, Q. Liu. Identification and analysis of twinning variants during compression of a Mg-Al-Zn alloy. Scripta Mater. 58 (2008) 122-125.

[36] É. Martin, L. Capolungo, L. Jiang, J.J. Jonas. Variant selection during secondary twinning in Mg-3%Al. Acta Mater. 58 (2010) 3970-3983.

[37] S. Wang, C. Schman, L. Bao, J.S. Lecomte, Y. Zhang, J.M. Raulot, M.J. Philippe, X. Zhao, C. Esling. Variant selection criterion for twin variants in titanium alloys deformed by rolling. Acta Mater. 60 (2012) 3912-3919.

[38] J. Lind, S.F. Li, R. Pokharel, U. Lienert, A.D. Rollett, R.M. Suter. Tensile twin nucleation events coupled to neighboring slip observed in three dimensions. Acta Mater. 76 (2014) 213-220.

[39] L. Capolungo, P.E. Marshall, R.J. McCabe, I.J Beyerlein, C.N. Tomé. Nucleation and growth of twins in Zr: a statistical study. Acta Mater. 57 (2009) 6047-6056.

[40] J.H. Cho, S.H. Kim, S.H. Han, S.B. Kang. Microstructure characterization of ZK60 magnesium alloy using TEM and HR-EBSD. Microsc Microanal. 19 (2013) 8-12.

[41] Y.L. Chen, L. Jin, J. Dong, Z.Y. Zhang, F.H. Wang. Twinning effects on the hot deformation behavior of AZ31 Mg alloy. Mater Charact. 118 (2016) 363-369.

[42] G.S. Song, Q.Q. Chen, S.H. Zhang, Y. Xu. Deformation micro-mechanism for compression of magnesium alloys at room temperature analyzed by electron backscatter diffraction. Mater. Des. 65 (2015) 534-542.

[43] Q. Li. Microstructure and deformation mechanism of 0001 magnesium single crystal subjected to quasi static and high-strain-rate compressive loading. Mater Sci Eng A. 568 (2013) 96-101.

[44] B. Syed, J. Geng, R.K. Mishra, K.S. Kumar. [0001] compression response at room temperature of single-crystal magnesium. Scripta Mater. 67 (2012) 700-703.

[45] X. Liu, J.J. Jonas, B.W. Zhu, T. Wang, L.X. Li. Variant selection of primary extension twins in AZ31 magnesium deformed at 400 ^{o}C. Mater Sci Eng A. 649 (2016) 461-467.

[46] Burke, E.C., Hibbard, W.R. Plastic deformation of magnesium single crystals. Trans. Metall. Soc. AIME 194 (1952) 295–303.

[47] Kelly, E.W., Hosford, W.F. Plane-strain compression of magnesium and magnesium alloy crystals. Trans. Metall. Soc. AIME 242 (1968) 5–13.

[48] R.E. Reed-Hill, W.D. Robertson. Additional modes of deformation twinning in magnesium. Acta Metall. 5 (1957) 717-727.

[49] R.E. Reed-Hill, W.D. Robertson. Deformation of magnesium single crystals by nonbasal slip. Trans. TMS-AIME. 220 (1957) 496-502.

[50] S.R Agnew, M.H. Yoo, C.N. Tomé. Application of texture simulation to understanding mechanical behavior of Mg and solid solution alloys containing Li or Y. Acta Mater. 49 (2001) 4277-4289.